J. Fluid Mech. (1996), *vol.* 324, *pp.* 333–353

Displacement of inviscid fluid by a sphere moving away from a wall

By I. EAMES[1], J. C. R. HUNT[2] AND S. E. BELCHER[3]

[1] Department of Applied Mathematics and Theoretical Physics, University of Cambridge, Silver Street, Cambridge CB3 9EW, UK

[2] Meteorological Office, Bracknell, Berks RG12 2SZ, UK

3 Department of Meteorology, University of Reading, Reading RG6 2AU, UK

(Received 11 October 1995 and in revised form 13 May 1996)

We develop a theoretical analysis of the displacement of inviscid fluid particles and material surfaces caused by the unsteady flow around a solid body that is moving away from a wall. The body starts at position h_S from the wall, and the material surface is initially parallel to the wall and at distance h_L from it. A volume of fluid D_{f+} is displaced away from the wall and a volume D_{f-} towards the wall. D_{f+} and D_{f-} are found to be sensitive to the ratio h_L/h_S. The results of our specific calculations for a sphere can be extended in general to other shapes of bodies.

When the sphere moves perpendicular to the wall the fluid displacement and drift volume D_{f+} are calculated numerically by computing the flow around the sphere. These numerical results are compared with analytical expressions calculated by approximating the flow around the sphere as a dipole moving away from the wall. The two methods agree well because displacement is an integrated effect of the fluid flow and the largest contribution to displacement is produced when the sphere is more than two radii away from the wall, i.e. when the dipole approximation adequately describes the flow. Analytic expressions for fluid displacement are used to calculate D_{f+} when the sphere moves at an acute angle α away from the wall.

In general the presence of the wall reduces the volume displaced forward and this effect is still significant when the sphere starts 100 radii from the wall. A sphere travelling perpendicular to the wall, $\alpha = 0$, displaces forward a volume $D_{f+}(0) = 4\pi a^3 h_L/3^{3/2}h_S$ when the marked surface starts downstream, or behind the sphere, and displaces a volume $D_{f+}(0) \sim 2\pi a^3/3$ forward when it is marked upstream or in front of the body. A sphere travelling at an acute angle away from the wall displaces a volume $D_{f+}(\alpha) \sim D_{f+}(0)\cos\alpha$ forward when the surface starts downstream of the sphere. When the marked surface is initially upstream of the sphere, there are two separate regions displaced forward and a simple cosine dependence on α is not found.

These results can all be generalized to calculate material surfaces when the sphere moves at variable speed, displacements no longer being expressed in terms of time, but in relation to the distance travelled by the sphere.

1. Introduction

A region of inviscid fluid is marked with some dye and a solid body is introduced. If the body then moves at a constant speed, dye close to where the body passes is

displaced forwards whereas dye far from the centreline is displaced backwards (see the experiments of Lance & Naciri 1992). It is now widely recognized that quantifying such displacement is the key to understanding and quantifying two-phase problems. In many cases the displacement due to the body is as important as its contribution to velocity fluctuations and diffusivity of the flow or to the pressure drop from its drag: for example, in boiling (Beer & Durst 1968) and gas/liquid flows in diverging and converging pipes (Kowe *et al.* 1992). Moving volumes with closed surfaces also occur in inhomogeneous fluids and are produced by regions of localized vorticity, such as Hill's spherical vortex. These moving volumes cause an irrotational flow in the surrounding fluid similar to that caused by moving bodies, and are instructive models for understanding the effects of heat and mass transfer by the outward ejection of vortical eddies from the wall region in turbulent flows.

Darwin (1953) examined fluid displacement by calculating the deformation of a large marked-fluid surface situated initially far upstream of the body and perpendicular to the direction in which the body travels. The flow around the body distorts the material surface, displacing fluid forward in regions close to where the body passes, and displacing fluid far from the body backward. Darwin (1953) defined the drift volume – a kinematic concept – to be the volume between the final and initial position of the marked surface. He then established that under certain conditions the drift volume is equal to the volume of fluid associated with the added mass of the body – a dynamic concept. This important result has been applied to the study of generation of vorticity by bodies moving in weakly sheared flow (Lighthill 1956; Auton 1987), and in novel experiments by Bataille, Lance & Marie (1991) to calculate the added mass of spherical bubbles. It is more usual to express the drift volume in terms of the added-mass coefficient, which is the ratio of the volume of fluid associated with the added mass to the body's volume. The added-mass coefficient of a sphere is $\frac{1}{2}$, and of a circular cylinder is 1.

In unbounded flow, the drift volume is critically dependent on how the drift volume is evaluated since the defining integral is not convergent. Questions of convergence were discussed by Darwin (1953) and Benjamin (1986), and recently Eames, Belcher & Hunt (1994) have shown that convergence is intimately related to the evaluation of fluid momentum in an unbounded region. Darwin's (1953) original result is obtained only when the marked surface is initially located far upstream of the body. The variation of the drift volume with the initial position of the marked surface was shown by Eames *et al.* (1994) to have a large effect on the volume of fluid displaced forward. For instance, when the marked surface is initially downstream of the body, the volume displaced forward may be larger, e.g. $\frac{3}{4}$ of the volume of a sphere, or 2 times the volume of a circular cylinder.

Studies of fluid displacement by a solid body moving in bounded geometry have been limited to a body travelling along an infinite channel, where the drift volume is equal to the negative of the body's volume. A simplification arises in this problem because the added mass is constant, and results from the analysis of displacement in unbounded flow are applicable. As with unbounded flow, fluid in the region close to where the body passes is displaced forward, but by the conservation of mass, there is a return flow due to the volume displaced forward and the volume of the body (see figure 1*a*). This leads to a negative displacement spread uniformly across the channel width.

In this paper we investigate fluid displacement by a solid body moving away from a wall, using for illustration the flow around a sphere (see figure 2). Two new aspects of the calculation are that the fluid particles are marked at arbitrary positions

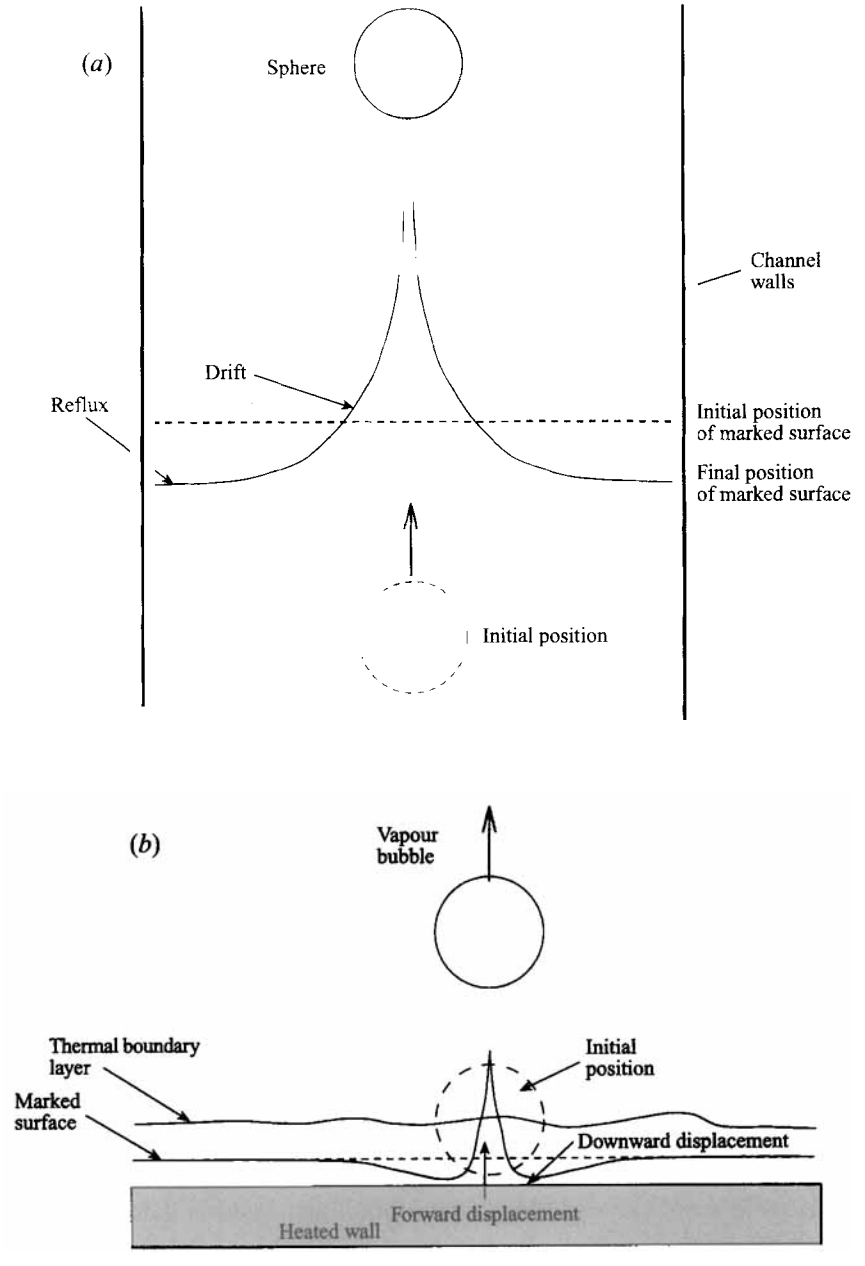

FIGURE 1. Schematic showing (*a*) fluid displacement in channel flow and (*b*) fluid displacement by a vapour bubble moving away from a wall. Material is carried across the thermal boundary layer.

relative to the sphere, and that the added mass of the body is time dependent. Lamb (1932) established that the added mass of the sphere increases close to the wall, and since added mass contributes to fluid drift we expect the presence of the wall to increase the volume of fluid displaced forward. However, the wall inhibits fluid motion perpendicular to the wall, thereby decreasing the volume of fluid displaced forward. Which of these effects dominates and why?

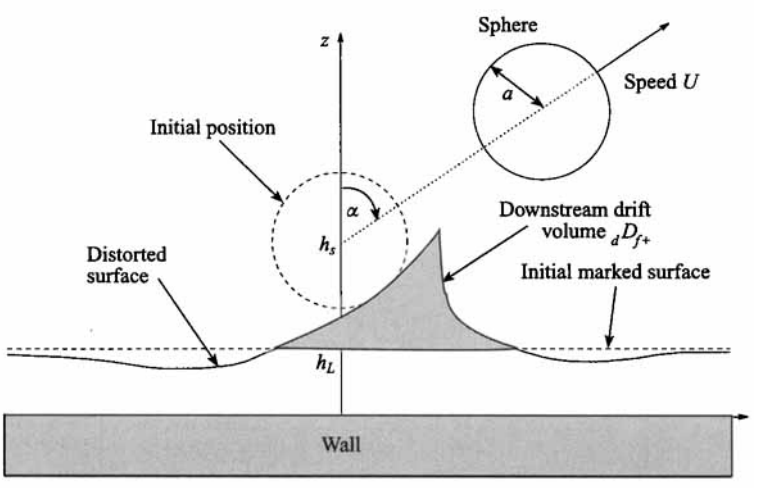

FIGURE 2. Distortion of a material surface by a sphere moving away from a wall.

We require a notation which refers to the initial position of the marked plane, and have adopted the following terminology: *upstream* and *downstream* refer to the initial position of the marked surface relative to the body, so that a surface marked upstream is initially in front of the body; following Darwin (1953), we refer to displacement forwards (in the direction of the body) as *drift*, and displacement backwards as *reflux*.

The paper is structured in the following way. In §2 the flow around a sphere moving away from a wall is calculated by expanding the velocity potential as an infinite series. The flow is approximated by truncating the series expansion after the first term and the displacement of a fluid particle is calculated in §3. The analytic approximation to displacement and drift volume is compared with the full numerical calculation when the sphere moves perpendicular to the wall. In §4, analytic expressions for displacement are integrated to evaluate the drift volume when the sphere travels away at an angle to the wall.

The results are likely to be of practical use in understanding 'nucleate boiling'. During boiling, vapour bubbles are generated on a heated plate and detach when the buoyancy force acting on them exceeds the surface tension force which keeps them anchored. As the bubbles detach and rise into the fluid bulk, they displace hot fluid into the colder ambient fluid leading to heat transfer (see figure 1*b*). The volume displaced forward through the thermal boundary layer is quickly mixed with the cooler ambient fluid, leading to an increase in heat transfer between the wall and fluid.

2. Potential flow due to a sphere moving away from a wall

The fluid flow, $\boldsymbol{v}_f$, around the sphere is assumed to be irrotational and so can be expressed in terms of the gradient of a scalar potential ϕ, $\boldsymbol{v}_f = \nabla\phi$, which from the continuity equation must satisfy Laplace's equation:

$$\nabla^2\phi = 0. \tag{2.1a}$$

Following Batchelor (1967, Chap. 6), the velocity field $\boldsymbol{v}_f$ is linearly related to the velocity of the sphere, $\boldsymbol{U}(t)$,

$$\phi(\boldsymbol{x}, t) = \sum \phi^{(n)}(\boldsymbol{x}; \boldsymbol{X}_s(t)) \boldsymbol{e}^{(n)} \cdot \boldsymbol{U}(t), \tag{2.1b}$$

where $\phi^{(n)}$ are the velocity potentials associated with the sphere moving at a unit speed in the direction of the unit vectors $\boldsymbol{e}^{(n)}$, and $\boldsymbol{X}_s(t)$ is the position of the body. The velocity potential of fluid around a sphere moving perpendicular to the wall, $\phi^{(1)}$, can be expressed in terms of an infinite series of dipoles, and this solution is well known (Lamb 1932). When the sphere is moving parallel to the wall, it is possible to express the velocity potential, $\phi^{(2)}$, in terms of an infinite series of multipoles, a solution recently derived by Kok (1993) and Li, Schultz & Merte (1993).

2.1. *Analytical solution*

Consider the incompressible inviscid flow around a sphere of radius a and at height h above a wall moving away from a wall at a constant speed U and at an angle α, as shown in figure 3. The z-axis is perpendicular the wall, and the sphere travels in the (z, x)-plane. The kinematic boundary conditions satisfied on the wall and sphere are

$$\frac{\partial \phi^{(n)}}{\partial z} = 0, \quad z = 0, \tag{2.2}$$

$$\frac{\partial \phi^{(1)}}{\partial r} = \cos\theta, \qquad \frac{\partial \phi^{(2)}}{\partial r} = \sin\theta \sin\varphi, \quad r = a, \tag{2.3a,b}$$

where (r, θ, φ) is the spherical coordinate system centred on A. Equation (2.3*a*) is the boundary condition due to the sphere moving at unit speed perpendicular to the wall and (2.3*b*) is due to the sphere moving with unit speed parallel to the wall.

By symmetry, the potential flow around the sphere moving away from the wall is identical to the flow around two spheres, A and B, moving apart (see figure 3). Defining a new spherical coordinate system centred on B as (r', θ', φ), the boundary condition which must be satisfied on B is

$$\frac{\partial \phi^{(1)}}{\partial r'} = -\cos\theta', \qquad \frac{\partial \phi^{(2)}}{\partial r'} = \sin\theta' \sin\varphi, \quad r' = a. \tag{2.4}$$

Calculation of flow around the sphere moving away from a wall reduces to solving the flow around two identical spheres travelling parallel at unit speed, and separating with unit speed.

The velocity potential of the flow around two separating spheres is well known and has been calculated using the method of images (Lamb 1932, p. 122), which generates a sequence of dipoles of suitable strengths and positions to satisfy the boundary conditions on both spheres. In Cartesian coordinates, the velocity potential due to two spheres separating with unit speed is

$$\phi^{(1)} = \sum_{i=0}^{\infty} \mu_i \left[-\frac{(z - a_i)}{(x^2 + y^2 + (z - a_i)^2)^{3/2}} + \frac{(z + a_i)}{(x^2 + y^2 + (z + a_i)^2)^{3/2}} \right], \tag{2.5}$$

where the recurrence relations for generating the position and strengths of the dipoles are $a_0 = h$, $a_1 = h - a^2/h$, $a_i = h - a^2/a_{i-1}$ and $\mu_0 = \frac{1}{2}a^3$, $\mu_i/\mu_{i-1} = a^3/a_{i-1}^3$.

The velocity potential of two spheres travelling parallel is calculated as an infinite series of multipoles rather than dipoles. (The method of images relies on the dipole pointing towards the centre of a sphere, and cannot be applied to calculate the

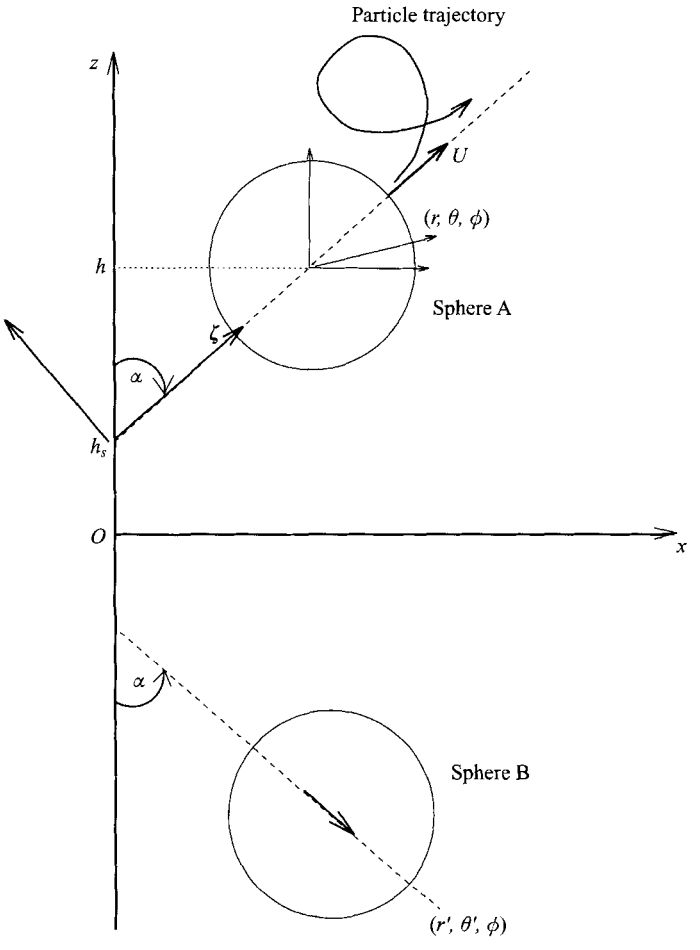

FIGURE 3. Notation for the calculation of the potential flow around spheres moving apart.

potential when the sphere is moving parallel to the wall.) The form of the potential is

$$\phi^{(2)} = \left(\frac{a^3}{2r^2} P_1^1(\cos\theta) + \frac{a^3}{2r'^2} P_1^1(\cos\theta') + \sum_{n=1}^{\infty} \left(\frac{a^{n+2}}{r^{n+1}} A_n P_n^1(\cos\theta) + \frac{a^{n+2}}{r'^{n+1}} B_n P_n^1(\cos\theta') \right) \right) \sin\varphi, \quad (2.6)$$

where the associate Legendre polynomials (Gradshteyn & Ryzhik 1980) are

$$P_1^1(\cos\theta) = \sin\theta, \quad P_2^1(\cos\theta) = 3\sin\theta\cos\theta, \quad P_3^1(\cos\theta) = \ldots. \quad (2.7)$$

There have been many attempts to calculate the coefficients, A_n and B_n, as an asymptotic expansion in a/h (Hicks 1880), but only recently (Kok 1993; Li *et al.* 1993) have recurrence relations for the coefficients A_n and B_n in terms of a/h been derived. Kok (1993) expanded the coefficients c_n in a series in a/h, which was evaluated to an accuracy of $(a/2h)^{50}$. Li *et al.* (1993) calculated the coefficients to be

$$A_n = (-1)^{n-1} c_n, \qquad B_n = c_n, \quad (2.8)$$

where

$$c_n = \frac{1}{2}\frac{n}{n+1}c^{n+2}\Big(1 + \sum_{i=1}^{\infty}\frac{i^2(i+n)!}{(n+1)!(i+1)!}c^{2i+1} + \sum_{i=1}^{\infty}\sum_{j=1}^{\infty}\frac{i^2(i+j)!}{(j+1)!(i+1)!}c^{2i+1}\frac{j^2(j+n)!}{(n+1)!(j+1)!}c^{2j+1} + \ldots\Big), \quad (2.9)$$

and $c = a/2h$.

When the sphere is close to the wall, a large number of terms need to be evaluated to get a good approximation to the flow, but far from the boundary (typically $h > 2.0a$), the fluid flow is dominated by the first terms of (2.5) and (2.6) which combine to give the velocity potential $\phi = U_1\phi^{(1)} + U_2\phi^{(2)} \sim \phi_A + \phi_B$, where the velocity potential of an isolated sphere A is

$$\phi_A \sim -\frac{1}{2}a^3U\frac{(x - Ut\sin\alpha)\sin\alpha + (z - h_S - Ut\cos\alpha)\cos\alpha}{((x - Ut\sin\alpha)^2 + y^2 + (z - h_S - Ut\cos\alpha)^2)^{3/2}}$$

and the velocity potential of B is

$$\phi_B \sim -\frac{1}{2}a^3U\frac{(x - Ut\sin\alpha)\sin\alpha - (z + h_S + Ut\cos\alpha)\cos\alpha}{((x - Ut\sin\alpha)^2 + y^2 + (z + h_S + Ut\cos\alpha)^2)^{3/2}}. \quad (2.10)$$

The velocity potential $\phi = U_1\phi^{(1)} + U_2\phi^{(2)}$ describes the flow around a sphere moving at a speed U_1 perpendicular to a wall, and at a speed U_2 parallel to the wall; the components can be written concisely as $U_i = \boldsymbol{e}^{(n)} \cdot \boldsymbol{U}(t)$. The speeds of spheres A and B are $U = (U_1^2 + U_2^2)^{1/2}$, and the angle at which sphere A moves away from the wall is $\tan\alpha = U_2/U_1$. The approximation $\phi \sim \phi_A + \phi_B$ describes the flow around two separating dipoles and is used in later sections to calculate analytic expressions for fluid displacement and the partial drift volume.

2.2. *Numerical evaluation*

The coefficients c_n given in (2.9) are required in the calculation of the flow around the sphere moving parallel to the wall and were evaluated numerically. These coefficients are expensive to evaluate because the summation is over many indices, and so we approximated them by truncating the series in (2.9) at the seventh term, and using Shank's transformation to accelerate convergence (see NAG Fortran Library). We obtain agreement to within 10% of the values of c_n tabulated in Li *et al.* (1993) and Kok (1993).

To determine the accuracy of truncating the series (2.5) and (2.6), we examined the fluid velocity on the surface of the sphere to see the degree to which the boundary conditions on the sphere are satisfied. We calculated the difference between the boundary condition on the sphere and that of the truncated velocity potential expansion in the $y = 0$ plane, firstly keeping the height of the sphere fixed and increasing the number of terms (figure 4*a*,*b*), and secondly fixing the number of terms and increasing the height above the wall (figure 4*c*,*d*). The conclusion from these calculations is that when the sphere is far from the wall, $h > 2.0a$, the flow is well described by the two-dipole approximation, with errors in satisfying the boundary conditions typically less than 10%. As h increases, the two-dipole approximation becomes a better approximation to the flow,

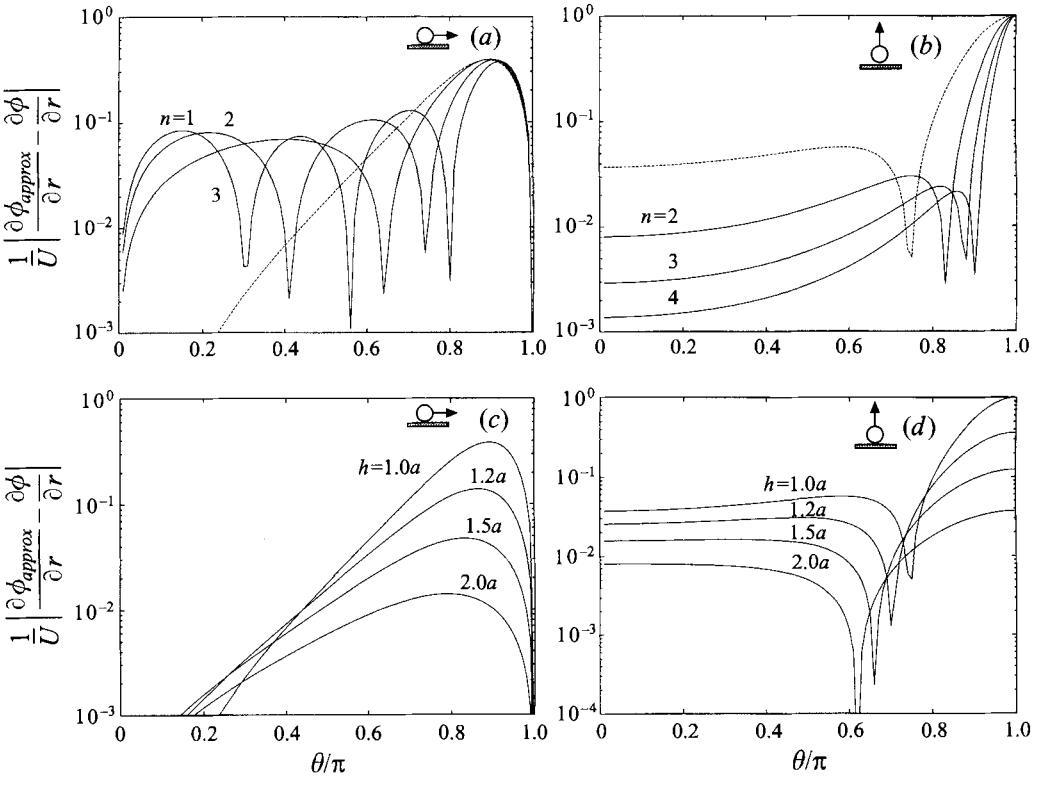

FIGURE 4. The error between the boundary condition on the sphere (2.3) and the value calculated by truncating the series expansion of the velocity potential after the n-th term, $|\partial\phi_{approx}/\partial r - \partial\phi/\partial r|/U$. In (*a*) and (*b*), the sphere is touching the wall ($h = 1.0a$), and the number of terms evaluated in the approximation is increased. The two-dipole approximation is plotted (· · · · · ·). In (*c*) and (*d*), the two-dipole approximation is used and h is increased. The sphere moves parallel to the wall (i.e. $\alpha = \pi/2$) in (*a*) and (*c*), but moves perpendicular to the wall (i.e. $\alpha = 0$) in (*b*) and (*d*).

and the error in satisfying the boundary conditions decreases. This result is central to establishing an analytic framework to calculate fluid displacement near a wall.

3. Fluid particle displacement

We consider the motion of a fluid particle initially marked at (x_0, y_0, h_L) in the Cartesian frame of reference. The marked fluid particle is displaced by the fluid motion to (x_f, y_f, z_f) in time t, where the vertical position of the fluid particle is given by

$$z_f(t) = h_L + \int_0^t \frac{\partial\phi}{\partial z}(x_f, y_f, z_f, t)\mathrm{d}t. \tag{3.1}$$

The fluid displacement depends only on the final and initial positions of the body and the trajectory between these two points, but not the speed of the body. For the specific case of a translating sphere, the vertical displacement can be calculated numerically by solving equation (3.1) using the series expansion of ϕ derived in the previous section. We calculate an analytic expression for fluid particle displacement, $z_f(t)$, by truncating the series expansion for ϕ after the first term.

3.1. *Analytical expression*

The displacement of the marked particle can be re-written as

$$z_f(t) = h_L + \int_0^t \frac{\partial \phi}{\partial z} \mathrm{d}t = h_L + \int_0^t \frac{\partial \phi_A}{\partial z}(x_f, y_f, z_f, t)\mathrm{d}t + \int_0^t \frac{\partial \phi_B}{\partial z}(x_f, y_f, z_f, t)\mathrm{d}t, \quad (3.2)$$

where ϕ_A and ϕ_B are the velocity potentials of the flow induced by spheres A and B respectively in the sense of (2.1*b*). We linearize (3.2) in the sense that the displacement due to two spheres is approximately equal to the sum of the displacements due to one sphere, in the absence of the other. The total displacement is approximately $z_f(t) \sim h_L + z_A(t) + z_B(t)$, where $z_A(t)$ is the fluid displacement due to sphere A in the absence of sphere B, and similarly for $z_B(t)$. We use expressions for the fluid displacement caused by the movement of an isolated sphere developed by Eames *et al.* (1994).

The displacement of a fluid particle along the z-axis due to sphere A is calculated by projecting the displacement, which lies primarily in the plane $z = x\cot\alpha + h_S$, on to the z-axis. We define the local coordinate system (ζ, η), with the origin at the initial position of the sphere, $\hat{\boldsymbol{\zeta}}$ a unit vector pointing in the direction in which sphere A travels and $\hat{\boldsymbol{\eta}}$, a unit vector perpendicular to $\hat{\boldsymbol{\zeta}}$. The marked particle has an initial position (ζ_0, η_0) in the (ζ, η) frame of reference, and (x_0, y_0, h_L) in the Cartesian frame; these coordinates are related by

$$\eta_0 = \left(y_0^2 + (x_0\cos\alpha + (h_S - h_L)\sin\alpha)^2\right)^{1/2},$$

and $\zeta_0 = x_0\sin\alpha + (h_L - h_S)\cos\alpha$. From figure 3 we see that the unit vector in the z-direction is $\hat{\boldsymbol{z}} = \cos\alpha\hat{\boldsymbol{\zeta}} + \sin\alpha\hat{\boldsymbol{\eta}}$, so that

$$\frac{\partial \phi_A}{\partial z} = \hat{\boldsymbol{z}} \cdot \nabla\phi_A = \cos\alpha\frac{\partial \phi_A}{\partial \zeta} + \sin\alpha\frac{\partial \phi_A}{\partial \eta}. \quad (3.3)$$

The fluid displacement in the z-direction due sphere A is

$$z_A(t) = \int_0^t \frac{\partial \phi_A}{\partial z}\mathrm{d}t = \int_0^t \nabla\phi_A \cdot \hat{\boldsymbol{z}}\mathrm{d}t = \cos\alpha\int_0^t \frac{\partial \phi_A}{\partial \zeta}\mathrm{d}t + \sin\alpha\int_0^t \frac{\partial \phi_A}{\partial \eta}\mathrm{d}t. \quad (3.4)$$

The first term on the right is the displacement of the fluid particle in the direction in which the sphere travels, which Eames *et al.* (1994) show is equal to

$$\int_0^t \frac{\partial \phi_A}{\partial \zeta}\mathrm{d}t = -\left[\frac{\phi_A}{U}\right]_0^t + \int_0^t \frac{q^2}{U}\mathrm{d}t, \quad (3.5)$$

where $q = |\nabla\phi_A|$. The asymptotic properties of Darwin's (1953) drift volume, $\int_0^\infty q^2/U\mathrm{d}t$, first calculated by Lighthill (1956), are restated here for the situation when the marked fluid element is initially in front of the sphere ($h_L > h_S + a$):

$$\int_0^t \frac{q^2}{U}\mathrm{d}t$$

$$\sim \begin{cases} \dfrac{9\pi a^6}{64\eta_0^5} + O\left(\dfrac{a^7}{\eta_0^5},\right) & \eta_0 \gg 2.5a, \quad (3.6a) \\[2ex] \dfrac{4a}{3}\left(1 + \dfrac{\eta_0^2}{3a^2}\right)\log\left(\dfrac{2a3^{3/4}}{\eta_0}\right) - 2a - \dfrac{\pi a}{3\sqrt{3}}\left(1 - \dfrac{\eta_0^2}{3a^2}\right) - \dfrac{\eta_0^2}{9a}, & \eta_0 \ll 0.17a. \quad (3.6b) \end{cases}$$

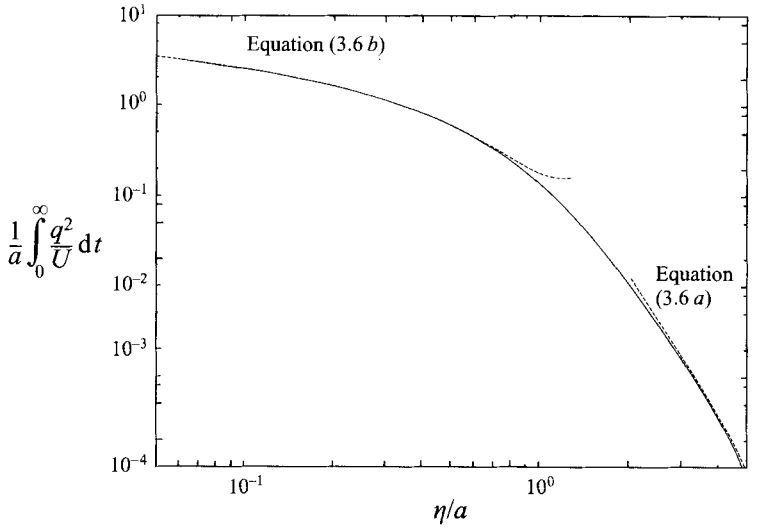

FIGURE 5. Numerical calculation of Darwin's drift (——) compared with the asymptotic expressions (3.6) (- - - -).

When the marked particle is initially behind the sphere (i.e. $h_L < h_S - a$),

$$\int_0^t \frac{q^2}{U}\mathrm{d}t \sim o\left(\frac{a^6}{\zeta_0^5}\right).$$

In the intermediate range $0.17a < \eta_0 < 2.5a$, $\int_0^\infty (q^2/U)\mathrm{d}t$ is calculated numerically, as shown in figure 5.

The second term on the right in (3.4) is the displacement along the η-axis. Now the initial and final values of η, namely η_0 and $\lim_{t\to\infty}\eta$, are not equal, but this contribution to the displacement is typically small and can be neglected. To see this, consider the second term in (3.4), namely

$$(\eta_0 - \lim_{t\to\infty}\eta)\sin\alpha. \tag{3.7}$$

In terms of the initial position it can be shown (see Eames *et al.* 1994, equation 2.30) that

$$\lim_{t\to\infty}\eta = \eta_0\left(1 - \frac{a^3}{(\eta_0^2+\zeta_0^2)^{3/2}}\right)^{1/2}. \tag{3.8}$$

When $\zeta_0 \gg \eta_0$, the contribution from (3.7) is of order

$$\sin\alpha\left(\frac{1}{2}a^3\frac{\eta_0}{(x_0^2+(h_L-h_S)^2+y_0^2)^{3/2}}\right), \tag{3.9}$$

which is negligible when the initial separation of the sphere and marked surface is large. The total fluid particle displacement caused by sphere A is approximately

$$z_A(t) \sim -\cos\alpha\left[\frac{\phi_A}{U}\right]_0^t + \cos\alpha\int_0^t \frac{|\nabla\phi_A|^2}{U}\mathrm{d}t. \tag{3.10}$$

Since sphere B moves away from all marked particles, the contribution from

$\int(|\nabla\phi_B|^2/U)\mathrm{d}t$ to the displacement is negligible and so

$$z_B(t) \sim \cos\alpha\left[\frac{\phi_B}{U}\right]_0^t. \tag{3.11}$$

The total displacement of a fluid particle along the z-axis, which is initially located at $z_f(0) = h_S$, is

$$z_f(t) \sim h_L + z_A(t) + z_B(t) \sim h_L - \cos\alpha\left[\frac{\phi_A - \phi_B}{U}\right]_0^t + \cos\alpha\int_0^t \frac{|\nabla\phi_A|^2}{U}\mathrm{d}t. \tag{3.12}$$

This expression is valid providing the sphere is more than two radii away from the wall. A comparison between (3.12) and a numerical calculation shows that (3.12) accurately predicts displacement even when the sphere is initially close to the wall. The specific form of the above equation is interesting since the third term on the right-hand side is always positive and is insensitive to the initial separation of the sphere and fluid particle ζ_0 (see 3.6*a*), in contrast to the second term which is sensitive to ζ_0 and may be positive or negative.

3.2. *Numerical calculation of fluid particle displacement*

When the sphere moves perpendicular to the wall, the displacement was calculated by solving (numerically)

$$\frac{\mathrm{d}x}{\mathrm{d}t} = \frac{\partial\phi}{\partial x}, \quad \frac{\mathrm{d}y}{\mathrm{d}t} = \frac{\partial\phi}{\partial y}, \quad \frac{\mathrm{d}z}{\mathrm{d}t} = \frac{\partial\phi}{\partial z}, \tag{3.13}$$

subject to the initial conditions $x = x_0$, $y = y_0$, $z = h_L$ at time $t = 0$. Since in this particular case the flow is axisymmetric, it is sufficient to fix $y_0 = 0$ and examine the displacement for positive x_0. The fluid velocity components were calculated numerically by truncating the series expansion of velocity potential (2.5) after a large number of terms. A comparison between the analytical approximation to displacement (3.12) and the numerical solution is shown in figure 6(*a,b*). Because of the difference in magnitude of positive and negative displacements they are plotted with different scales – a logarithmic scale for positive displacement and a linear scale for negative displacement. Figure 6(*a,b*) shows that the region displaced forward is a circle centred on the z-axis and that the deformed surface cuts the plane $z_f = h_L$ at one point. The agreement between the numerical solution and the analytic approximation for displacement is good despite the sphere being initially located close to the wall. This is at first surprising since the analytic approximation to displacement is based on the two-dipole approximation, which is not an adequate description when the sphere is close to the wall (see figure 4*b*). However the integrated effect of the fluid flow on the fluid displacement means that the main contribution comes from when the body is far from the wall, i.e. when $h > 2.0a$, where the two-dipole approximation is a good description of the flow.

The accuracy of the analytical expression to describe displacement, when the sphere moves *perpendicular* to the wall, suggests that the same approach should be applicable when the sphere moves at an acute angle *away* from the wall. Figure 6(*c,d*) shows only the analytic expression for displacement plotted for fixed values of the initial position of the sphere and marked surface, but with varying angles at which the sphere moves away from the wall. The origin of each of the curves plotted in figure 6(*c,d*) is different; the abscissa is now $x - (h_L - h_S)\tan\alpha$. Also, the horizontal range is chosen to coincide with the scale on figure 9, where the regions of positive displacement are

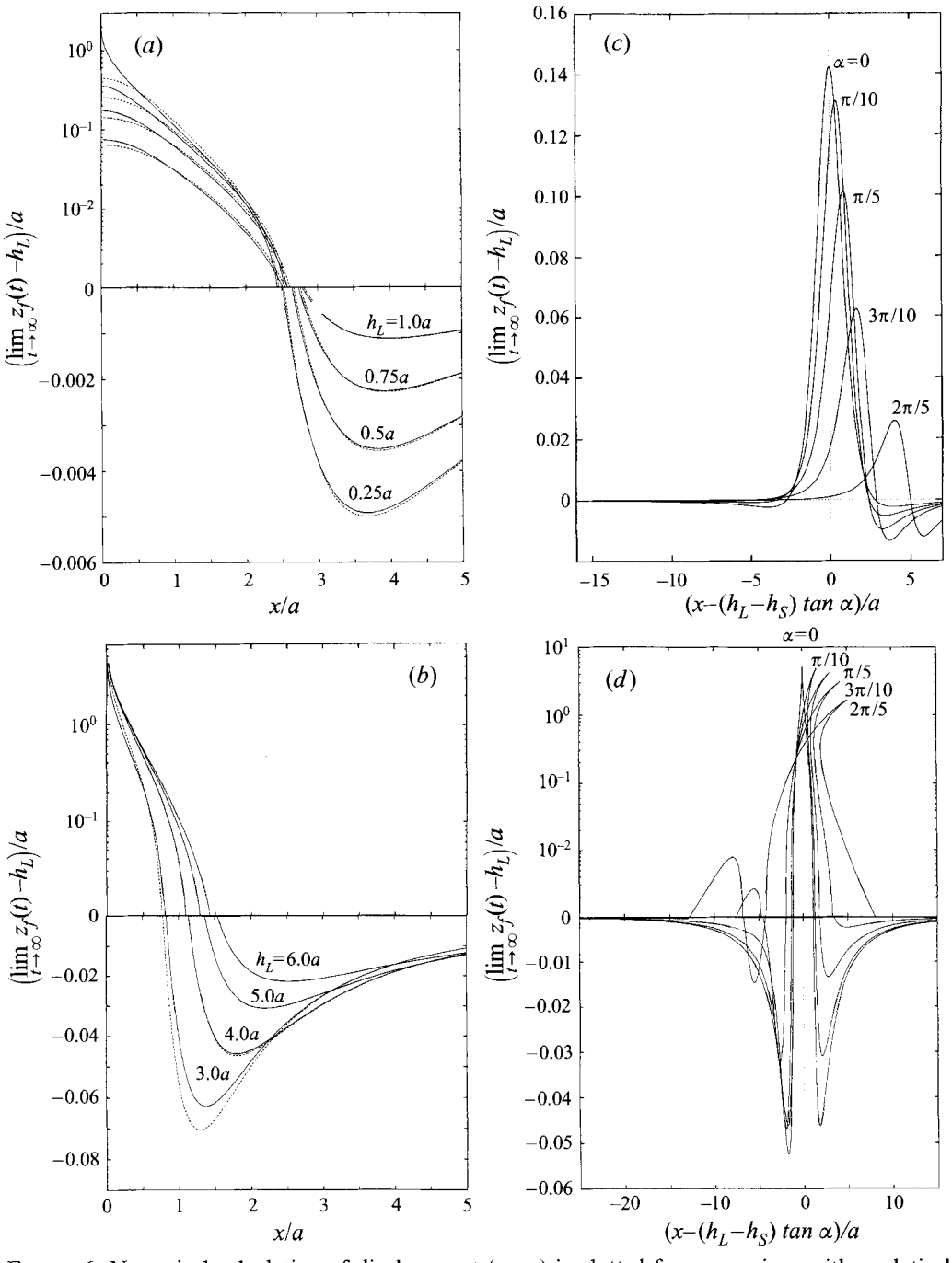

FIGURE 6. Numerical calculation of displacement (——) is plotted for comparison with analytical approximations (· · · · · ·) (3.12). Note, in (*a*) and (*b*) we plot the graphs with a logarithmic scale on the positive vertical axes, and with a linear scale on the negative axes; consequently we see a discontinuity in the graph (see main text). In both (*a*) and (*b*) the sphere is initially at $h_S = 2.0a$ and moving perpendicular to the wall; the marked surface is either initially in front of the sphere, as in (*b*) where $h_L = 3.0a, 4.0a, 5.0a, 6.0a$), or behind the sphere, as in (*a*) where $h_L = 0.25a, 0.5a, 0.75a, 1.0a$. Only analytic expressions for displacement are plotted in (*c*) and (*d*) when the sphere moves at an angle away from the wall. In both (*c*) and (*d*) the initial position of the marked surface and sphere are fixed ($h_S = 2.0$ and $h_L = 0.5a$ in *c*) and ($h_S = 2.0a$, $h_L = 4.0a$ in *d*). The angle at which the sphere moves away from the wall is varied $\alpha = 0, \frac{1}{10}\pi, \frac{1}{5}\pi, \frac{3}{10}\pi, \frac{2}{5}\pi$

plotted. We see clearly that one effect of the acute angle of ejection is that the fluid displacement is reduced.

A significant difference which arises when the sphere moves at an acute angle to the wall is that there may be two regions where fluid is displaced forward, as seen in figure 6(*d*) and 9(*b*). As we shall see in the next section, this gives rise to an extra contribution to upstream drift volume.

4. Partial drift volume in the presence of a solid boundary

4.1. *Definition*

The *fluid partial drift volume*, D_f, was defined by Eames *et al.* (1994) to be the volume of fluid between the final and initial position of a finite-sized marked surface, which is initially a finite distance from the body. For instance, the partial drift volume associated with a circular disk of radius R_0 and height h_L above the wall is

$$D_f(R_0) = \int_0^{2\pi} \int_0^{R_0} (\lim_{t\to\infty} z_f(t) - h_L) R \, \mathrm{d}R \, \mathrm{d}\varphi, \tag{4.1}$$

where $\lim_{t\to\infty} z_f(t)$ is the ultimate position of a fluid particle initially marked on the disk.

Using the notation defined in the introduction, we refer to the volume of fluid displaced *forward*, away from the wall (see figure 2), as the *drift volume*, D_{f+}, defined by

$$D_{f+} = \int_0^{2\pi} \int_0^{\infty} \max\left(\lim_{t\to\infty} z_f(t) - h_L, 0\right) R \, \mathrm{d}R \, d\varphi. \tag{4.2}$$

Likewise, the volume of fluid displaced backwards is referred to as the *reflux volume*, D_{f-}, and can be related to D_{f+} by

$$D_{f-} = \lim_{R_0\to\infty} D_f(R_0) - D_{f+}. \tag{4.3}$$

In both cases, the term is prefixed by *up/downstream* depending on whether that material surface is initially marked upstream or downstream of the body. Where appropriate, the symbols D_{f+}, D_{f-} are prefixed by subscript u or d. By calculating the partial drift volume associated with a large disk, $\lim_{R_0\to\infty} D_f(R_0)$, we can reduce the problem of calculating the volume displaced backwards and forwards to just the calculation of D_{f+}; the up/downstream reflux volume is then given through the relation (4.3).

4.2. *Asymptotic expressions for partial drift volumes when the marked plane is large*

The partial drift volume associated with a marked circular plane of radius R_0 is evaluated using (4.1) and (3.12) to give

$$D_f(R_0, \alpha) = \cos\alpha \int_0^{2\pi} \int_0^{R_0} \left[\frac{\phi_A - \phi_B}{U}\right]_{t=0} R \, \mathrm{d}R \, \mathrm{d}\varphi + \cos\alpha \int_0^{R_0} \int_0^{t} \frac{q^2}{U} \mathrm{d}t \, 2\pi R \, \mathrm{d}R. \tag{4.4}$$

The partial drift volume thus has two contributions: the first is related to the momentum and the second to the kinetic energy of the fluid. The first is more sensitive to the initial separation between the sphere and marked surface than the second. The magnitude of the second term decays rapidly away from the sphere. The first term on the right-hand side may be evaluated by changing the order of

integration:

$$\int_0^{R_0}\int_0^{2\pi}\left[\frac{\phi_A-\phi_B}{U}\right]_{t=0}\mathrm{d}\varphi\, R\,\mathrm{d}R$$
$$\sim \pi a^3\cos\alpha\left(\frac{1}{(1+(R_0/h_L+h_S)^2)^{1/2}}-\frac{1}{(1+(R_0/h_L-h_S)^2)^{1/2}}\right), \tag{4.5}$$

when $h_L < h_S - a$, and

$$\int_0^{R_0}\int_0^{2\pi}\left[\frac{\phi_A-\phi_B}{U}\right]_{t=0}\mathrm{d}\varphi\, R\,\mathrm{d}R$$
$$\sim \pi a^3\cos\alpha\left(-2+\frac{1}{(1+(R_0/h_L-h_S)^2)^{1/2}}+\frac{1}{(1+(R_0/h_L+h_S)^2)^{1/2}}\right), \tag{4.6}$$

when $h_L > h_S + a$. The second term on the right-hand side of (4.5) can be approximated by

$$\int_0^{2\pi}\int_0^{R_0}\int_0^{\infty}\frac{q^2}{U}\mathrm{d}t\, R\,\mathrm{d}R\,\mathrm{d}\varphi \sim \tfrac{2}{3}\pi a^3 - O\left(\frac{3\pi^2 a^6}{32R_0^3}\right), \tag{4.7}$$

when $h_L > h_S + a$, where $\frac{2}{3}\pi a^3$ is the drift volume of a sphere (Darwin 1953). Combining (4.5) and (4.7), we find that the partial drift volume associated with a large marked plane is

$${}_dD_f(R_0,\alpha) \sim \pi a^3\cos^2\alpha\left(\frac{1}{(1+(R_0/h_L+h_S)^2)^{1/2}}-\frac{1}{(1+(R_0/h_L-h_S)^2)^{1/2}}\right) \tag{4.8}$$

when the surface is downstream of the sphere, and

$${}_uD_f(R_0,\alpha) \sim \pi a^3\cos^2\alpha\left(\frac{1}{(1+(R_0/h_L+h_S)^2)^{1/2}}+\frac{1}{(1+(R_0/h_L-h_S)^2)^{1/2}}\right)$$
$$-2\pi a^3\cos^2\alpha+\tfrac{2}{3}\pi a^3\cos\alpha \tag{4.9}$$

when the surface is upstream.

From (4.8) and (4.9) we see that the partial drift volume is a quadratic function of the new variable $\cos\alpha$. The first factor of $\cos\alpha$ is expected because the displacement lies primarily along the ζ-axis, which is projected onto the z-axis. The second $\cos\alpha$ factor arises from reflux which depends on the initial position of the plane; drift is insensitive to the initial position of the plane and does not contribute to a second $\cos\alpha$ factor.

There are four length scales: $h_L - h_S$, h_S, R_0 and a, so that three dimensionless variables R_0/h_S, $(h_S - h_L)/a$, and R_0/a determine the solution. We concentrate on those limits which lead to relationships between the reflux and drift volumes (4.3). For a small radius

$$\lim_{R_0/h_S\to 0}{}_uD_f(R_0) \sim \tfrac{2}{3}\pi a^3\cos\alpha, \tag{4.10}$$

whereas for a large radius

$$\lim_{R_0/h_S\to\infty}{}_uD_f(R_0) \sim -2\pi a^3\cos^2\alpha+\tfrac{2}{3}\pi a^3\cos\alpha, \tag{4.11}$$

which means that more fluid is brought in towards the wall. When the surface is marked downstream of the sphere,

$$\lim_{R_0/h_S\to 0}{}_dD_f(R_0) \sim \pi a^3\cos^2\alpha \tag{4.12}$$

and

$$\lim_{R_0/h_S\to\infty} {}_dD_f(R_0) \sim \pi a^3 O\left(\frac{h_L h_S}{R_0^2}\right). \tag{4.13}$$

The above analysis can be generalized to the calculation of the partial drift volume of an arbitrarily shaped two- or three-dimensional body moving away from a wall, where the dipole strength in unbounded flow is prescribed (Eames 1995).

4.3. *Analytic expression for the up/downstream drift volume when the sphere moves perpendicular to the wall*

We have seen in figure 6(*a,b*), that when the sphere moves perpendicular to the wall the flow is axisymmetric and the marked surface cuts the plane $z_f = h_L$ at one radial position, $R = R_f$. The fluid displaced forward is contained within the region $R < R_f$, whereas the fluid displaced backwards is outside this region and so the drift and reflux volumes can be written succinctly as

$$D_{f+} = D_f(R_f), \quad D_{f-} = \lim_{R_0/h_S\to\infty} D_f(R_0) - D_{f+}. \tag{4.14}$$

The partial drift volume associated with a large surface depends on the initial location of the marked surface relative to the sphere (from (4.10) and (4.11)):

$$\lim_{R_0/h_S\to\infty} {}_uD_f(R_0) = 0, \qquad h_L < h_S - a, \tag{4.15a}$$

$$\lim_{R_0/h_S\to\infty} {}_dD_f(R_0) = -\tfrac{4}{3}\pi a^3, \qquad h_L > h_S + a. \tag{4.15b}$$

Given D_{f+}, we can evaluate D_{f-} directly using (4.14) and (4.15). The radial position, $R = R_f$, can be calculated by solving the equation $\lim_{t\to\infty} z_f(t) = h_L$. When the surface is marked downstream of the sphere, $h_L < h_S - a$, a fluid particle with zero displacement satisfies

$$\lim_{t\to\infty} z_f(t) \sim h_L + \frac{(h_S - h_L)a^3}{2((h_S - h_L)^2 + R_f^2)^{3/2}} - \frac{(h_S + h_L)a^3}{2((h_S + h_L)^2 + R_f^2)^{3/2}} = h_L. \tag{4.16}$$

There are two interesting cases to examine: firstly when the wall effect is negligible ($h_L \sim h_S - a$), and secondly when it is significant ($h_L \ll h_S$). Under these two limits, it can be shown from (4.16) that

$$R_f \sim \begin{cases} 2^{1/3} h_S^{1/3} \left(h_S^2 - h_L^2\right)^{1/3}, & h_L \lesssim h_S - a \\ \sqrt{2} h_S + O\left(h_L^2/h_S\right), & h_L \ll h_S. \end{cases} \tag{4.17}$$

The downstream drift volume is calculated using the expression for R_f, (4.17), substituted into (4.9):

$${}_dD_{f+} \sim \begin{cases} \pi a^3 \left(1 - \dfrac{3}{2}\left(\dfrac{h_S - h_L}{2h_S}\right)^{2/3}\right), & h_L \lesssim h_S - a \\ \pi a^3 \dfrac{4}{3^{3/2}} \dfrac{h_L}{h_S}, & h_L \ll h_S. \end{cases} \tag{4.18}$$

The above equation tells us that when $h_S \sim 100a$, the largest value of ${}_dD_{f+}$ differs by 10% from its value calculated in unbounded flow, namely πa^3, which shows the significant long-range effect of the wall.

The variation of the drift volume with the location of the surface, h_L, can be

estimated from displacement along the centreline,

$$\lim_{t\to\infty} z_f(t) \sim \int_0^\infty U\left(\frac{a^3}{(Ut-h_S+h_L)^3}-\frac{a^3}{(Ut+h_S+h_L)^3}\right)\mathrm{d}t \sim \frac{2a^3h_L}{h_S^3}.$$

The volume can be estimated by calculating the region of radius R_f which experiences a positive fluid velocity. In unbounded flow $R_f^2 < 2(h_S-h_L)^2 \sim 2h_S^2$, and so in this case the radius of the region displaced forward is $R_f \sim \sqrt{2}h_S$, agreeing with (4.17). The volume displaced forward is ${}_dD_{f+} \sim 2a^3h_L/h_S^3 \times \pi R_f^2 \sim 4\pi a^3(h_L/h_S)$. This simple argument shows how the downstream drift volume varies with h_L, agreeing with (4.18). However the coefficient is over-estimated because the average displacement is much less than $2a^3h_L/h_S^3$.

When the marked surface is upstream of the sphere, $h_L > h_S+a$, the radial position R_f is obtained by solving

$$\lim_{t\to\infty} z_f(t) \sim h_L - \frac{(h_L-h_S)a^3}{2((h_L-h_S)^2+R_f^2)^{3/2}} - \frac{(h_L+h_S)a^3}{2((h_L+h_S)^2+R_f^2)^{3/2}} + \int_0^\infty \frac{q^2}{U}\mathrm{d}t \sim h_L. \quad (4.19)$$

An asymptotic solution for R_f can be generated when $2.5a \ll R_f \ll h_L - h_S$, using a binomial expansion of (4.19) in R_f and an asymptotic approximation to $\int(q^2/U)\mathrm{d}t$, (3.6*a*), is used to show

$$R_f \sim \left(\frac{9\pi(h_L^2-h_S^2)^2a^3}{64(h_L^2+h_S^2)}\right)^{1/5}, \quad 2.5a \ll R_f \ll h_S - h_L, \quad (4.20)$$

from which the upstream drift volume can be calculated:

$${}_uD_{f+} \sim \tfrac{2}{3}\pi a^3 - \tfrac{7}{6}\pi a^3\left(\frac{9\pi}{64}\right)^{2/5}\left(\frac{(h_L^2-h_S^2)a^2}{(h_S^2+h_L^2)^2}\right)^{3/5}, \quad 2.5a \ll R_f \ll h_S - h_L. \quad (4.21)$$

The upstream drift volume slowly approaches the value calculated by Darwin (1953) in unbounded flow, $\frac{2}{3}\pi a^3$, as the initial height of the sphere increases.

Comparing (4.18) and (4.21) shows paradoxically that a body can transport more material away from the wall when the initial position of the material surface is downstream and closer to the wall, than when it starts upstream of the body and far from the wall. The reason is that there is a return flow due to the body moving away from the wall, (4.15*b*), which reduces the volume displaced forward, $\frac{2}{3}\pi a^3$, when the surface is upstream of the body. There is no return flow of fluid when a surface is initially located downstream, (4.15*a*), and so the drift volume is typically larger, ${}_dD_{f+} \sim \pi a^3$. This suggests that vapour bubbles formed above the surface transport more heat away from the wall than those formed close to the wall!

4.4. *Numerical calculations of the partial drift volume*

When the sphere moves perpendicular to the wall, D_{f+} was also calculated numerically by following a large number of fluid particles. The radius, R_f, was estimated by linearly extrapolating between a fluid particle displaced forwards and the adjacent particle which is displaced backwards. The up/downstream drift volume was calculated by integrating the displacement over a circular disk of radius R_f centred on the z-axis. Figures 7 and 8 show a comparison between the numerical solution of R_f and D_{f+} and the analytic approximations. Analytic expressions for R_f (4.17) and D_{f+} (4.18) are plotted for $h_L < h_S - a$. When $h_L > h_S + a$, the region displaced forward is calculated by first solving (4.19) numerically for R_f, and the upstream drift volume is

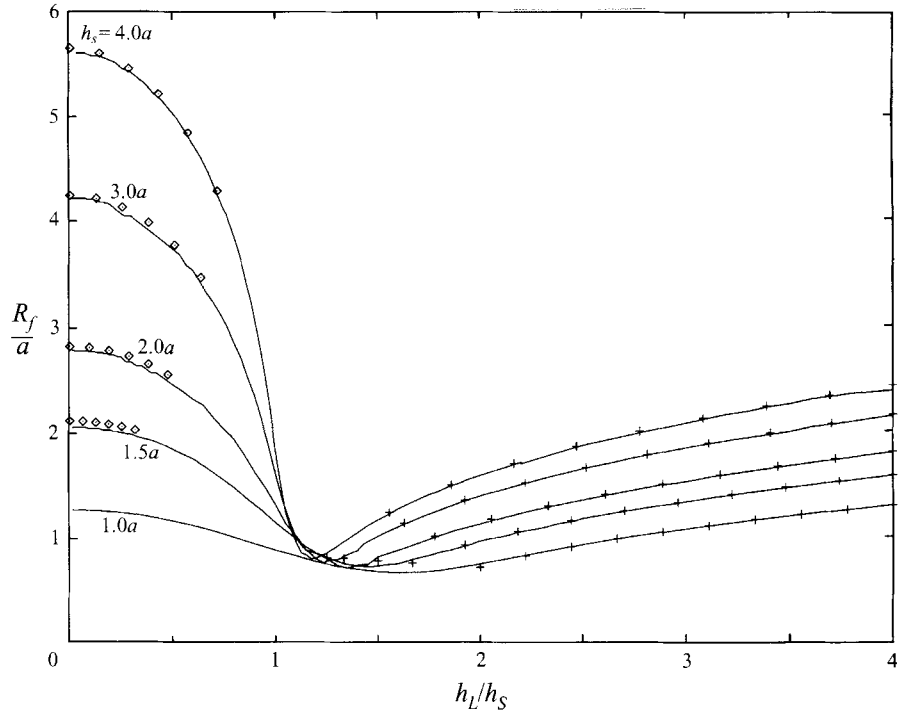

FIGURE 7. Radius of the region displaced forward (R_f) when the sphere moves perpendicular to the wall. The numerical solutions (——) are plotted for comparison with the analytical expressions (4.17) ($\diamond$) for $h_L < h_S - a$, and with a numerical solution of (4.19) for $h_L > h_S + a$ (+). The initial height of the sphere, h_S/a is varied: 1.0,1.5,2.0,3.0,4.0.

evaluated using a combination of analytic expressions to calculate the first term on the right-hand side of (4.4) and numerical integration to evaluate the second term. Both figures show a good agreement between the numerical and analytical solutions when the sphere moves perpendicular to the wall, where the analytical expressions are based on the two-dipole approximation of the fluid flow.

The analytical expressions for displacement were used to calculate D_{f+} when $\alpha > 0$. Firstly, the region of fluid displaced forward was calculated from (3.12) and the results are shown in figure 9. A striking difference between the distortion of a material surface when the sphere travels at an acute angle away from the wall and travels perpendicular to the wall is that an additional region of fluid is displaced forward (see figure 9*b* with $\alpha = 2\pi/5$).

Displacement is integrated over the regions plotted in figure 9, in order to evaluate D_{f+}, which is shown in figure 10(*a*,*b*). The accuracy of the analytic expressions for displacement depends on the integrated effect of the flow on displacement, so that a sphere travelling at a steep angle spends more time closer to the wall, in the region where the dipole approximation does not adequately describe the flow. For this reason we have limited our attention to $\alpha < 0.4\pi$. On first inspection we might expect that since $D_f \sim \cos^2\alpha$ the downstream drift volume to will vary as ${}_dD_{f+} \sim \cos^2\alpha$. However, the numerical results show that ${}_dD_{f+}$ varies more closely with $\cos\alpha$. This is because as the volume of the region in which fluid is displaced forward increases, the average displacement decreases. Therefore $\int(\phi/U)\mathrm{d}A$ is independent of α, and ${}_dD_{f+} \sim \cos\alpha \int(\phi/U)\mathrm{d}A$ varies as $\cos\alpha$.

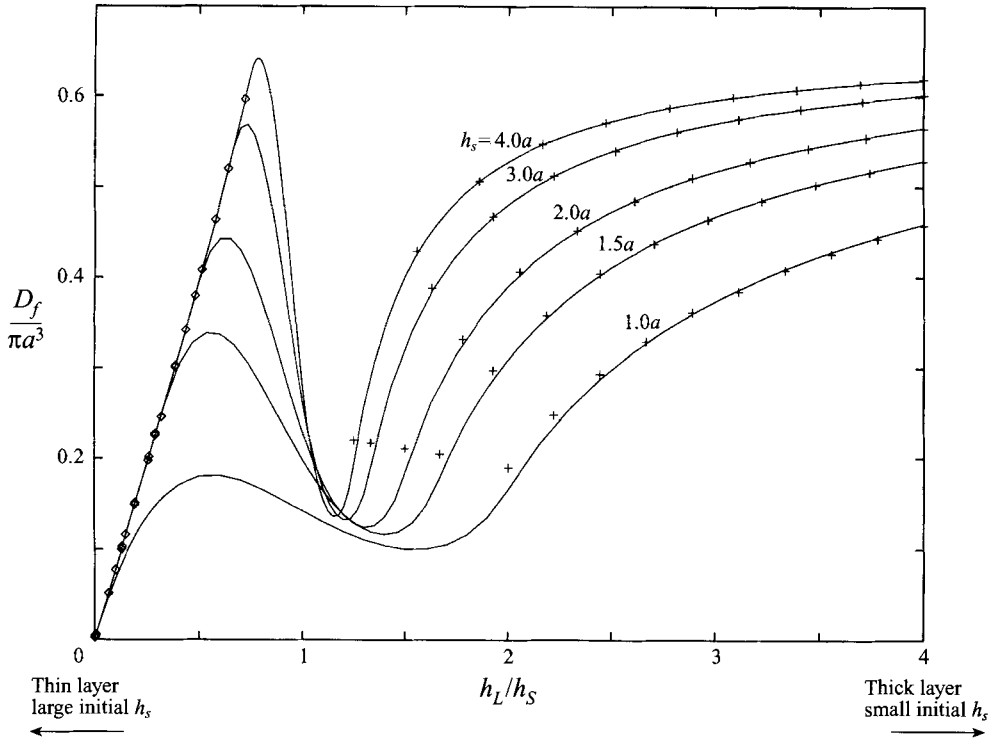

FIGURE 8. Volume of fluid displaced forward, D_{f+}, when the initial height of the sphere h_S is varied relative to initial position of sphere: $h_S/a = 1.0, 1.5, 2.0, 3.0, 4.0$. The full numerical solution is shown by ——. Analytical expressions for D_{f+} (4.18) plotted for $h_L < h_S - a$ as ◇. For $h_L > h_S + a$, the approximation (+) is obtained by integrating the expression for displacement (3.12) using a combination of analytical and numerical methods.

In contrast, we would have expected the upstream drift volume to vary like $\cos\alpha$, but figure 10(*b*) shows that this agreement is poor. The regions of principle drift and reflux no longer overlap and the two regions are displaced forward (figure 9*b*). The area of the regions increases and so $\int\int(q^2/U)\mathrm{d}t\mathrm{d}A$ increases. Therefore we would expect $D_{f+}(\alpha)/D_{f+}(0)$ to be larger than the $\cos\alpha$ variation, which is indeed the case. There is no secondary region when $\alpha < 0.26\pi$ and the contribution to ${}_uD_{f+}$ from the secondary region is 10% when $\alpha \sim 0.3\pi$. These values are for $h_L = 4.0a$ and $h_S = 2.0a$.

5. Conclusion

We have calculated an analytic expression for the displacement of fluid by a sphere moving away from a wall, which we have tested by comparing with numerical solutions when the sphere moves perpendicular to the wall. Comparisons between the numerical solution and analytic expressions show good agreement despite the sphere starting close to the wall. The analytic expression for displacement is integrated numerically to calculate the drift volume when the sphere moves at an oblique angle away from the wall. We also find that the downstream drift volume shows a cosine dependence on the ejection angle, ${}_dD_{f+}(\alpha) \sim {}_dD_{f+}(0)\cos\alpha$.

We have seen that the dynamic and kinematic effects of the wall on the flow associated with a sphere are different. Although the added mass of the sphere is

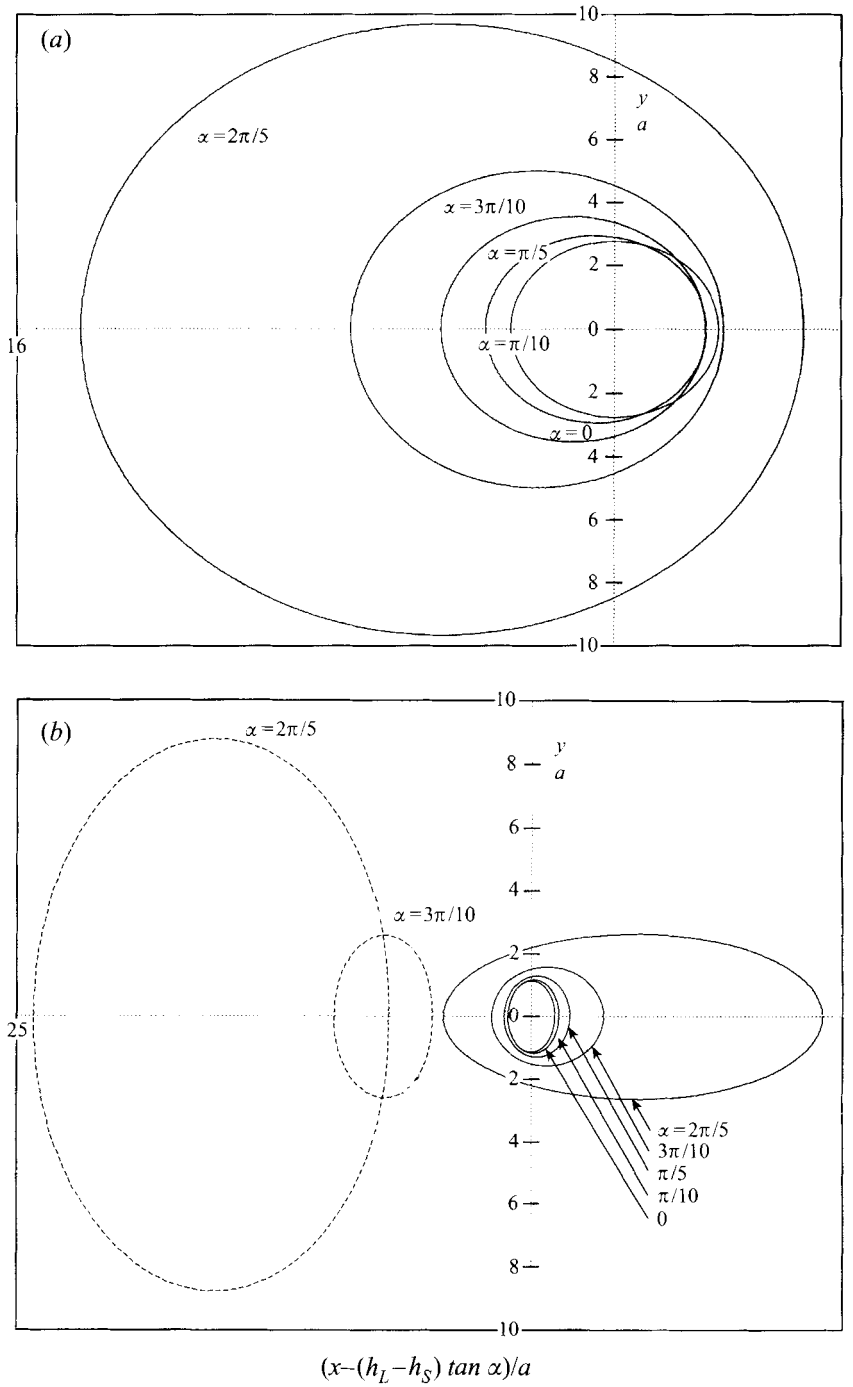

FIGURE 9. The boundaries separating the region of positive and negative drift is plotted for different angles at which the sphere moves away from the wall (α) when (*a*) the sphere is initially in front of the marked surface $h_S = 2.0a$, $h_L = 0.5a$ and (*b*) the sphere is initially behind the marked surface $h_S = 2.0a$, $h_L = 4.0a$. The solutions are calculated by solving numerically the analytical expressions for the particle displacement (3.12). See figure 6(*c*,*d*) for comparison. Note the secondary region in (*b*).

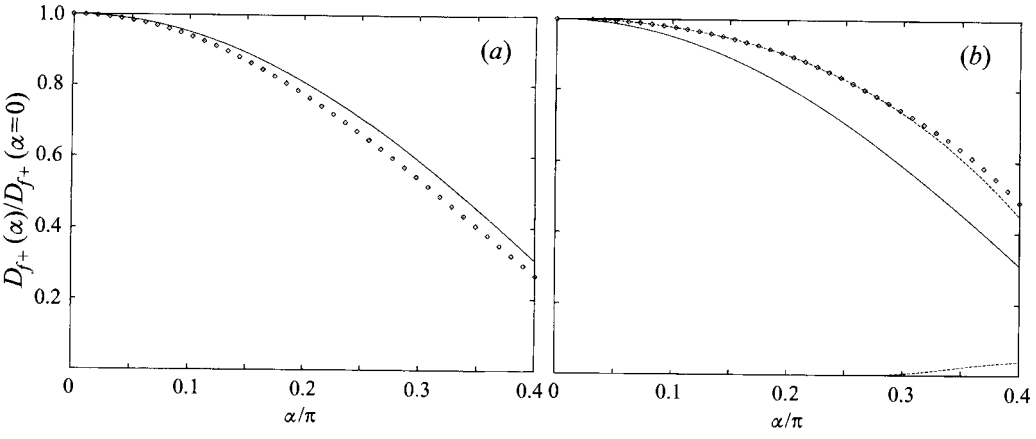

FIGURE 10. Volume of material displaced forward for arbitrary angle $D_{f+}(\alpha)$ ($\diamond$) is plotted against α when (a) the surface is downstream of the sphere ($h_S = 2.0$, $h_L = 0.5a$), and (b) when the surface is initially upstream of the sphere ($h_S = 2.0$, $h_L = 4.0$). For comparison, the function $\cos\alpha$ is plotted (——). In (b), the contributions from the two regions displaced forward are plotted (- - - -), the lower curve represents the contribution from the region bounded by – – – in figure 9(b).

larger near the wall (i.e. more force is required to accelerate it), it decreases quickly away from the wall, as $\frac{1}{2}(1 + O(a^3/h_S^3))$ (Lamb 1932), as it tends to its value of $\frac{1}{2}$ in unbounded flow. On the other hand, the kinematic boundary condition on the wall has an opposite effect, reducing the normal displacement and the volume displaced forward decreases due to the presence of the wall. Furthermore there is a difference in how far the wall effect extends. The dynamical effect of the wall rapidly decays from the wall like $O(a^3/h_S^3)$; the kinematic effect of the wall extends much further with a slower decay of D_{f+} like $(a/h_S)^{6/5}$. The result of the competition between the wall effects is a decrease in the drift volume.

We have shown that the volume displaced forward is sensitive to the initial location of the marked surface h_L/h_S, and surprisingly that more fluid can be displaced forward when the sphere starts far from the wall, than when the sphere starts close to the wall. The return flow required by the conservation of mass is significantly larger when the marked surface is initially upstream rather than downstream of the sphere.

The specific calculations in this paper for a sphere can be extended to other bodies by treating the body as a dipole of prescribed strength. In addition the added mass of the body is required which can be calculated from the body's volume and dipole strength (see Eames 1995). This description will not be accurate for a body initially close to the wall. The results can be applied to the calculation of fluid displacement and drift volumes due to a body travelling at an arbitrary speed along a straight trajectory since the fluid displacement is independent of the speed of the body and dependent only on the final and initial position of the body. The results for z_f, D_{f-} and D_{f+} derived here in terms of time can be re-expressed in terms of the equivalent time t^* defined in terms of the displacement of the sphere, $t^* = X_s/U_0 = 1/U_0 \int_0^t U(t)\mathrm{d}t$, where U_0 is the characteristic speed. This may be relevant for the problem of bubble and sand particle motion near walls.

In the context of heat transfer, the wall effect is obviously important. For instance, Beer & Durst (1968) used Darwin's concept of drift to examine heat transfer by bubbles near heated walls, but ignored the effect of the wall and so overestimated

the effect of the bubbles. As we have shown Darwin's (1953) relation between added mass and drift volume does not apply in these inhomogeneous flows.

I.E. gratefully acknowledges the sponsorship of BNFL through a CASE award, and support through the Jeremy Howarth Fellowship at St. Catharine's College.

REFERENCES

AUTON, T. R. 1987 The lift force on a spherical body in a rotational flow. *J. Fluid Mech.* **183**, 199–218.

BATAILLE, J., LANCE, M. & MARIE, J. L. 1991 Some aspects of the modelling of bubbly flows. In *Phase-Interface Phenomena in Multiphase Flow* (ed. G. F. Hewitt, F. Mayinger & J. R. Riznic), 179–193.

BATCHELOR, G. K. 1967 *An Introduction to Fluid Dynamics.* Cambridge University Press.

BEER, H. & DURST, F. 1968 Mechanismen der Wärmeübertraguag beim Blasenieden und inhre Simulation. *Chem. Ing. Tech.* **40**, 632–640.

BENJAMIN, T. B. 1986 Note on added mass and drift. *J. Fluid Mech.* **169**, 251–256.

DARWIN, C. 1953 Note on hydrodynamics. *Proc. Camb. Phil. Soc.* **49**, 342–354.

EAMES, I. 1995 Displacement of material by a solid body moving away from a wall. PhD thesis, Cambridge University.

EAMES, I., BELCHER, S. E. & HUNT, J. C. R. 1994 Drift, partial drift and Darwin's proposition. *J. Fluid Mech.* **254**, 201–223.

GRADSHTEYN, I. S. & RYZHIK, I. M. 1980 *Table of Integrals, Series, and Products*, 4th Edn. Academic.

HICKS, W. M. 1880 On the motion of two spheres in a fluid. *Phil. Trans. R. Soc. Lond.* **171**, 455–470.

KOK, J. B. W. 1993 Dynamics of a pair of gas bubbles moving through liquid. Part 1. Theory. *Eur. J. Mech.* B/*Fluids* **12**, 515–540.

KOWE, R., HUNT, J. C. R., HUNT, A., COUET, B. & BRADBURY, L. J. S. 1988 The effects of bubbles on the volume fluxes and the presence of pressure gradients in unsteady and non-uniform flow of liquids. *Intl J. Multiphase Flow* **14**, 587–606.

LAMB, H. 1932 *Hydrodynamics.* Cambridge University Press.

LANCE, M. & NACIRI, A. 1992 Added mass and lift coefficient of a single bubble. *1st European Fluid Mechanics Conference.* Cambridge.

LI, L., SCHULTZ, W. W. & MERTE, H. 1993 The velocity potential and the interacting for two spheres moving perpendicularly to the line joining their centers *J. Engng Maths* **27**, 147–160.

LIGHTHILL, M. J. 1956 Drift. *J. Fluid Mech.* **1**, 31–54 (and Corrigendum **2**, 311–312).